Available online at www.sciencedirect.com
SCIENCE DIRECT®
Journal of Catalysis 224 (2004) 178–186
JOURNAL OF CATALYSIS
www.elsevier.com/locate/jcat

Mesoporous H-GaMCM-48: A remarkable solid acid catalyst for tertiary butylation of phenol

S.E. Dapurkar and P. Selvam *

Department of Chemistry, Indian Institute of Technology-Bombay, Powai, Mumbai 400 076, India

Received 5 June 2003; revised 26 February 2004; accepted 26 February 2004

Abstract

A mesoporous gallosilicate (GaMCM-48) molecular sieve having a silicon-to-gallium (molar) ratio of 60 was synthesized hydrothermally, and the structure, coordination geometry of gallium, acidic properties, and catalytic activity were investigated systematically employing various analytical and spectroscopic techniques. XRD, TEM, and N_2 sorption investigations show a MCM-48 structure with highly ordered (meso)porosity. ^{71}Ga MAS-NMR studies reveal that gallium substitutes isomorphously in the mesoporous silicate framework of MCM-48. Further, NH_3-TPD profiles suggest the presence of a high concentration of moderate-to-strong Brønsted acid sites in H-GaMCM-48. The catalytic performance of this protonated catalyst was evaluated for the *t*-butylation of phenol reaction. The results indicate that the H-GaMCM-48 catalyst is highly active for the chosen reaction and shows a much higher substrate conversion than many other catalyst systems. However, compared to the analogous H-GaMCM-41, the H-GaMCM-48 shows only a slight decrease in *p*-*t*-butyl phenol selectivity owing to the formation of 2,4-di-*t*-butyl phenol. On the other hand, the deactivation is very minimal on account of the three-dimensional pore system of MCM-48 structure compared to the one-dimensional pore opening of the MCM-41 structure.

Keywords: GaMCM-48; Mesoporous; Molecular sieves; Tertiary butyl phenol; Alkylation

1. Introduction

The discovery of thermally stable mesoporous silicate molecular sieves [1] having one-dimensional hexagonal MCM-41 and three-dimensional cubic MCM-48 structures has attracted significant research interest, and opened up new opportunities in many areas, in particular, heterogeneous catalysis [2–6]. However, much attention has been devoted to the catalytic properties of the metal-containing MCM-41 structure because of the ease in preparation of these materials, and only very little attention has been paid to the catalytic properties of the metal-incorporated MCM-48 structure [7–10] owing to the difficulty in the synthesis of good quality samples due to a narrower homogeneity region of the MCM-48 phase [11]. On the other hand, the inherent benefit of the three-dimensional pore structure of MCM-48 as well as the associated advantage of the resistance against pore blockage of this phase could serve as an excellent candidate for catalytic applications. Furthermore, the three-dimensional pore opening of MCM-48 is also promising as it entails more agitated flow, which in turn increases the number of interactions between reactants and catalytic sites than the corresponding one-dimensional pore opening of MCM-41 [7,12–18]. For example, the isopropylation of napthalene and pyrene over AlMCM-48 exhibits much higher activity than AlMCM-41 [19]. However, it is noteworthy here that only a very few reports are available on the catalytic properties of mesoporous gallosilicates [9,10, 20–24]. Therefore, in this investigation, an attempt has been made to synthesize and characterize high-quality GaMCM-48, and to test its catalytic ability for the *tertiary*-butylation (*t*-butylation) reaction of phenol as the products, viz. *para-tertiary*-butyl phenol (*p*-*t*-BP) and 2,4-di-*tertiary*-butyl phenol (2,4-di-*t*-BP), are industrially important [25]. In addition, like many other porous solid acid catalysts, e.g., HY [26], ZSM-12 [27], SAPO-11 [28], H-AlMCM-41 [29,30], H-FeMCM-41 [31], H-GaMCM-41 [32], and H-AlMCM-48 [16], the mesoporous H-GaMCM-48 also possesses moderate acidic sites which is expected to favor the chosen reaction (Scheme 1). For a comparative study, we have also included

* Corresponding author. Fax: +91-22-2572-3480.
E-mail address: selvam@iitb.ac.in (P. Selvam).

0021-9517/$ – see front matter
doi:10.1016/j.jcat.2004.02.033

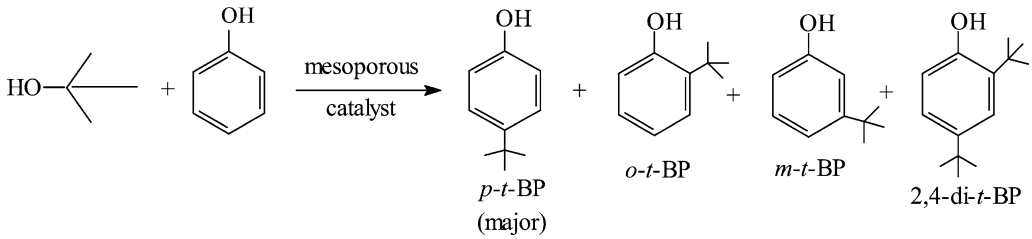

Scheme 1.

the results of B, Al, Ga, and Fe-containing MCM-41 as well as B, Al, and Fe-containing MCM-48 catalysts.

2. Experimental

2.1. Starting materials

Gallium nitrate nonahydrate ($Ga(NO_3)_3{\cdot}9H_2O$; Aldrich; 98%), tetraethylorthosilicate (TEOS; Aldrich; 98%), and cetyltrimethylammonium bromide (CTAB; Aldrich; 99%) were used as sources for gallium, silicon, and template, respectively, and sodium hydroxide (NaOH; Loba; 98%) was used as alkali source. Phenol (Merck; 99.5%) and *tertiary*-butyl alcohol (*t*-BA; Thomas Baker; 99%) were used for (vapor phase) phenol alkylation reactions. Authentic samples of *ortho-tertiary*-butyl phenol (*o-t*-BP; Fluka; 99%), *meta-tertiary*-butyl phenol (*m-t*-BP; Aldrich; 99%), *para-tertiary*-butyl phenol (*p-t*-BP; Fluka; 99%), and 2,4-di-*tertiary*-butyl phenol (2,4-di-*t*-BP; Fluka; 99%) were used for a comparative analyses of the reaction products.

2.2. Synthesis of GaMCM-48

The sodium form of GaMCM-48 was synthesized as per the following procedure with a typical molar gel composition of SiO_2:$0.25(Na_2O)_2$:$0.30(CTA)_2O$:$60H_2O$:$0.0083Ga_2O_3$. Initially, a solution A was obtained by mixing NaOH and tetraethyl orthosilicate in distilled water under constant stirring for 10 min. Another solution B was also prepared by dissolving CTAB in distilled water and was stirred for 20 min. Finally, a homogeneous transparent gel was obtained by mixing the solutions, viz. A and B under constant stirring for 25 min. In this resulting gel, gallium source was added and stirred further for 1 h for homogenization and the pH of the final gel was 11.4. This was then subjected to hydrothermal treatment at 383 K for 72 h. The solid as-synthesized product was washed repeatedly, filtered and dried at 353 K for 12 h, and calcined at 823 K for 2 h in N_2 followed by air for 6 h. For a comparison, gallium-free MCM-48 and AlMCM-41, FeMCM-41, GaMCM-41, AlMCM-48, FeMCM-48, BMCM-41, and BMCM-48 were prepared according to procedures described elsewhere [16, 28–34].

2.3. Preparation of H-GaMCM-48

The protonated form of GaMCM-48 was prepared from the calcined sample by an ion-exchange method. At first, NH_4-GaMCM-48 was obtained by repeated exchange of Na-GaMCM-48 with 1 M NH_4NO_3 solution at 353 K for 6 h. The H-GaMCM-48 was then obtained by deammoniation at 823 K for 6 h in air.

2.4. Characterization

All the samples were systematically characterized by powder X-ray diffraction (XRD; Rigaku), N_2 sorption isotherms (Sorptomatic-1990), simultaneous thermogravimetry-differential thermal analysis (TG-DTA; Shimadzu DT-30), Fourier transform-infrared (FT-IR; Nicolet Impact 400) spectroscopy, ^{29}Si and ^{71}Ga magic-angle spinning-nuclear magnetic resonance (^{29}Si MAS-NMR, Varian VXR-300S; and ^{71}Ga MAS-NMR, Bruker Avance DPX 300), and inductively coupled plasma-atomic emission spectroscopy (ICP-AES; Labtam Plasma 8440) techniques. The surface area was estimated using the Brunauer–Emmett–Teller (BET) method and the pore size was calculated by the Barrett–Joyner–Halenda (BJH) formula [35]. The pore volume was determined from the amount of N_2 adsorbed at $P/P_0 = 0.5$. TEM and ED analysis was carried out on a Philips CM 200 operating at 200 kV (structural resolution of 0.23 nm). The image and ED were recorded with a GATAN CCD camera. Calcined GaMCM-48 samples were used for TEM and ED studies. The sample was dispersed in ethanol with sonication (Oscar ultra sonics) and was placed a drop of it on a carbon-coated grid (300 mesh; Sigma-Aldrich).

2.5. Temperature-programmed desorption of ammonia

The acidic behavior of the H-GaMCM-48 catalyst was studied by temperature-programmed desorption of ammonia (NH_3-TPD). For this purpose, about 200 mg of H-GaMCM-48 was placed in a quartz reactor and was activated at 823 K in air for 6 h followed by 2 h in helium with a flow rate of 50 ml min^{-1}. The reactor was then cooled to 373 K and maintained for another hour under the same conditions. At this temperature, ammonia adsorption was carried out by passing the gas through the sample for about 20 min. Subsequently, it was purged with helium for an hour to remove the physisorbed ammonia. Finally, the desorption of ammonia was carried out by heating the reactor up to 823 K at

10 K min $^{-1}$. The amount of ammonia desorbed was estimated with the aid of a thermal conductivity detector response factor for ammonia.

2.6. Tertiary-butylation of phenol

The *t*-butylation reaction of phenol was carried out using 750 mg of H-GaMCM-48 catalyst in a homemade fixed-bed flow reactor. Prior to the reaction, the catalyst was activated at 773 K in flowing air for 8 h followed by cooling to reaction temperature (448 K) under nitrogen. After an hour, the reactant mixture, i.e., phenol and *t*-butyl alcohol, with a desired (molar) ratio and weight hour space velocity (WHSV) was fed into the reactor using a liquid injection pump (Sigmamotor) with nitrogen as carrier gas. The gaseous products obtained were cooled and the condensed liquid products were collected at 30-min intervals.

2.7. Products analyses

The various products of the *t*-butylation reaction, viz. *o*-*t*-BP, *m*-*t*-BP, *p*-*t*-BP, and *2,4*-di-*t*-BP, were identified by gas chromatography (Nucon 5700) with SE-30 and AT1000 columns. In addition, all these products were confirmed with the use of a combined gas chromatography-mass spectrometry (GC-MS; Hewlett G1800A) setup fitted with a HP-5 capillary column.

3. Results and discussion

Fig. 1 shows the XRD patterns of various GaMCM-48 samples. The diffraction patterns show all the major reflections, which are characteristic of a cubic mesoporous MCM-48 structure [1]. The calculated average unit cell parameter (a_0) for GaMCM-48 is 86.0 Å, which is higher than the gallium-free siliceous MCM-48 (80.2 Å). The increase in unit cell dimension could be attributed to the isomorphous substitution of trivalent gallium to tetravalent silicon owing to the larger crystal radius of the former (0.62 Å) than the latter (0.40 Å) [36]. Indeed, a similar unit cell expansion was also observed for AlMCM-48 [16] as well as FeMCM-48 [34]. The ICP-AES analysis of GaMCM-48 indicates that the gallium content (Si/Ga = 62) in the catalyst remains nearly the same or close to the starting (gel) composition (Si/Ga = 60), suggesting a complete incorporation of gallium in the silicate matrix.

Fig. 2 depicts the N_2 adsorption–desorption isotherms of GaMCM-48 showing type IV isotherm, which is a typical characteristic of mesoporous materials [37]. A sharp inflection in the relative pressure (P/P_0) range 0.2–0.4 corresponds to capillary condensation within uniform mesopores. The inset shows the BJH plot of the derivative of the pore volume per unit weight with respect to the pore diameter (dV/dD) versus the pore diameter. The pore volume, surface area, and pore diameter deduced from the N_2 adsorption isotherm for GaMCM-48 samples were 0.80 cm^3 g^{-1}, 1167 m^2 g^{-1}, and 32 Å, respectively. Similarly, the N_2 sorption analysis on the catalyst after reaction shows the type IV isotherm with capillary condensation in the range of relative pressure from 0.2 to 0.4. The pore volume, surface area, and pore diameter measured from the N_2 adsorption isotherm for catalysts after reaction were 0.74 cm^3 g^{-1}, 1020 m^2 g^{-1}, and

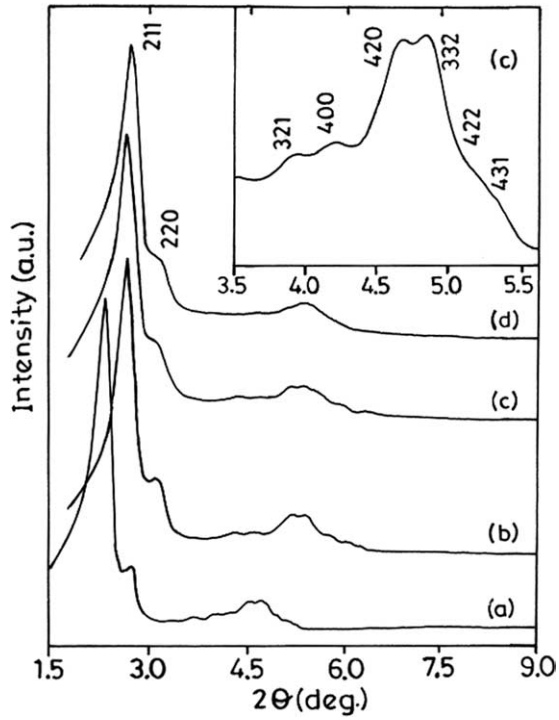

Fig. 1. XRD patterns of: (a) as-synthesized GaMCM-48, (b) calcined GaMCM-48, (c) H-GaMCM-48 before reaction, and (d) H-GaMCM-48 after reaction.

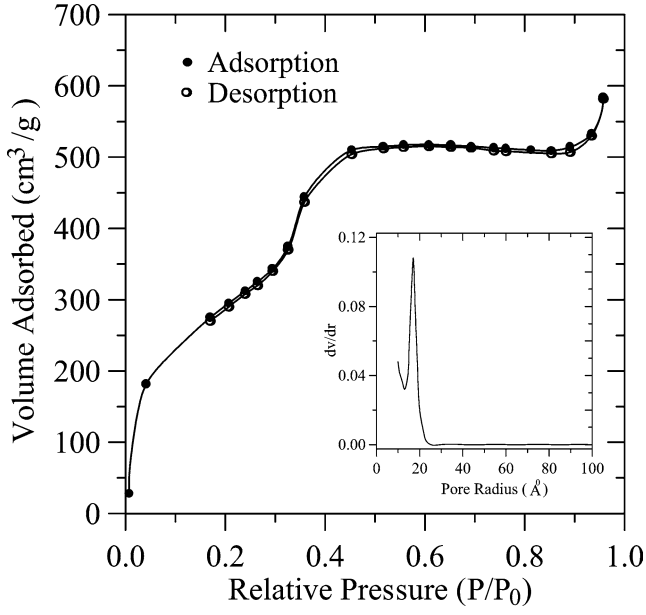

Fig. 2. N_2 adsorption–desorption isotherms of calcined GaMCM-48. The inset shows pore-size distribution.

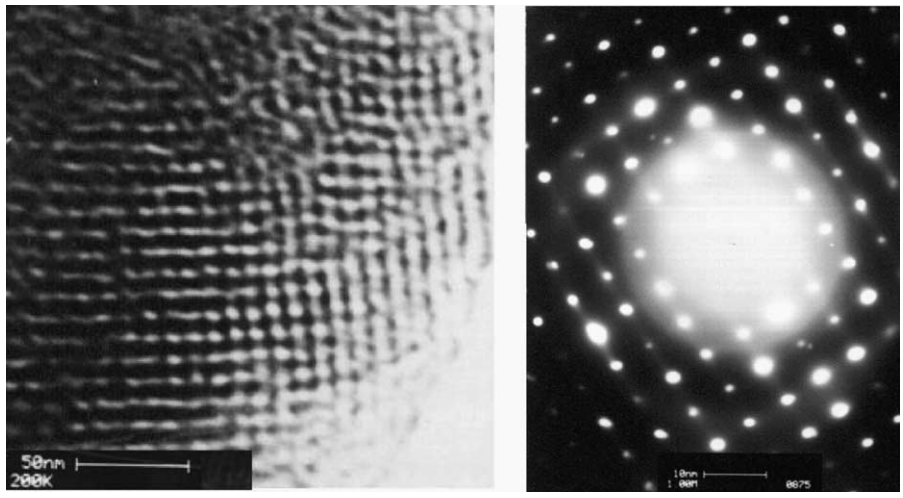

Fig. 3. TEM image and ED of calcined GaMCM-48.

29 Å, respectively. These results clearly support the mesoporous nature of the GaMCM-48 catalyst before and after reaction. The TEM image of calcined GaMCM-48 (Fig. 3a) indicates that the mesopores are arranged along the (110) plane [38], and that the ED pattern (Fig. 3b) confirms the good quality of the sample [39].

The TG of the as-synthesized Na-GaMCM-48 (not reproduced here) shows a total weight loss of about 55–60% (in three steps), which is typical of a mesoporous MCM-48 phase [9]. The observed (three) different weight losses correspond to the removal of adsorbed water and/or gas molecules (< 373 K; 5–7%), oxidative degradation of template molecules (393–725 K; 45–47%), and condensation (dehydroxylation) of silanol groups (> 773 K; 5–6%). This is well supported by the respective endothermic and/or exothermic transitions in DTA (also not reproduced here). On the other hand, TG of calcined Na-GaMCM-48 gives a 25% weight loss (Fig. 4,a). However, in the case of H-GaMCM-48 before (Fig. 4,b) and after (Fig. 4,c) reaction, a weight loss of 20–22% was noted. The corresponding endothermic transitions at 353 K, for the calcined sample, and 363 K, for the sample after reaction, confirm the desorption process. The observed weight loss as well as the endothermic transition of the calcined and the protonated samples could be attributed to the removal of adsorbed water and/or gaseous molecules occluded within the mesopores of GaMCM-48. These results indeed reveal the hydrophilic nature of GaMCM-48.

Fig. 5 presents the FT-IR spectra of various GaMCM-48 samples. It can be seen from this figure that there is no appreciable change in spectral features before (Fig. 5,c) and after reaction (Fig. 5,d), as compared to both the as-synthesized (Fig. 5,a) and calcined (Fig. 5,b) samples, suggesting the intactness of the mesoporous MCM-48 structure. This observation is well supported by the measured pore volume, pore diameter, and surface area of the same before and after the reaction run. The pore volume, pore diameter, and surface area of the catalyst before reaction gave values of 0.80 $cm^3\,g^{-1}$, 1167 $m^2\,g^{-1}$, and 32 Å, respectively, while

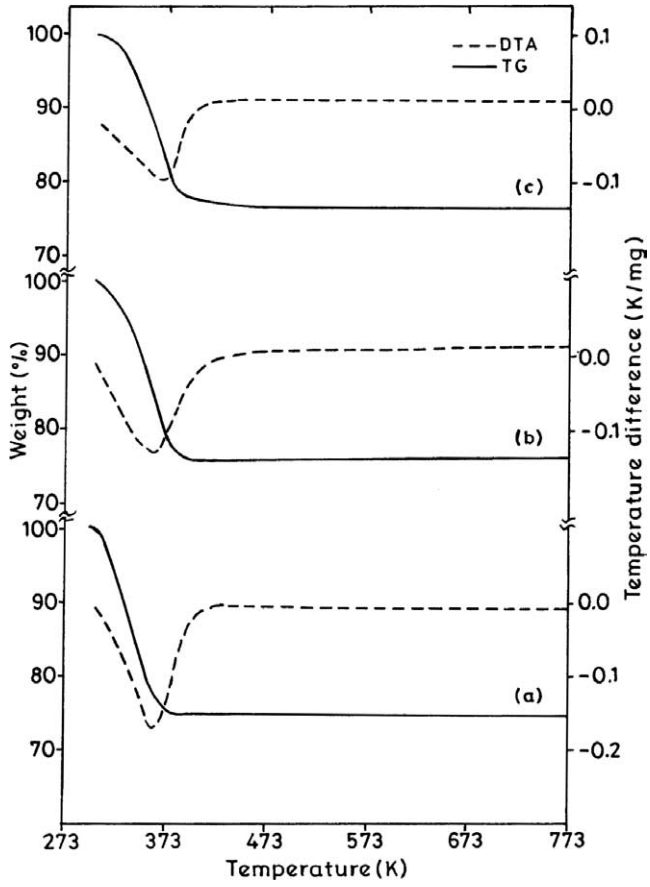

Fig. 4. TG-DTA spectra of: (a) calcined GaMCM-48, (b) H-GaMCM-48, and (c) H-GaMCM-48 after reaction and calcined (solid line TG, dashed line DTA).

for the catalyst after reaction the pore volume, pore diameter and surface area values were found to be 0.74 $cm^3\,g^{-1}$, 29 Å, and 1020 $m^2\,g^{-1}$, respectively. The broad bands in the region 3200–3800 cm^{-1} are assigned to surface hydroxyl groups. On the other hand, the bands at 2920 and 2848 cm^{-1} are characteristic of hydrocarbon moieties, which dis-

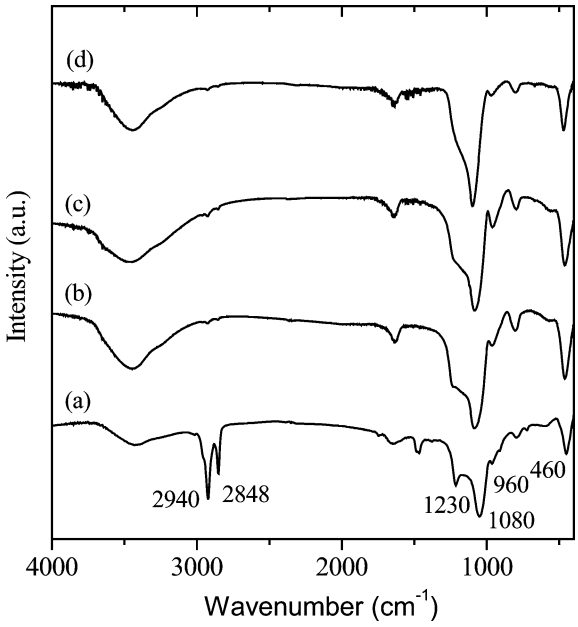

Fig. 5. FT-IR spectra of: (a) as-synthesized GaMCM-48, (b) calcined GaMCM-48, (c) H-GaMCM-48, and (d) H-GaMCM-48 after reaction and calcined.

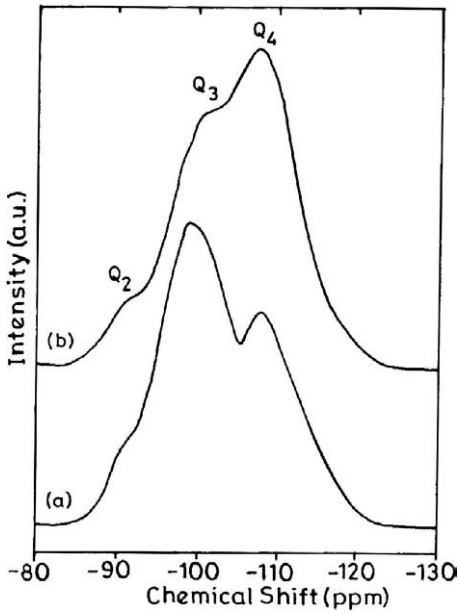

Fig. 6. ^{29}Si MAS-NMR spectra of: (a) as-synthesized GaMCM-48 and (b) calcined GaMCM-48.

appear upon calcination, indicating the removal of template molecules from the structure. The bands at 1230, 1080, and 460 cm^{-1} are assigned to symmetric stretching and bending of ≡Si–O–Si≡ vibrations while the weak bands at ∼960 cm^{-1} are attributed to defect sites (≡Si–OH) [17,40]. On the other hand, the Si–O$^-$ and Ga–O$^-$ stretching bands appear nearly in the same region (800–1100 cm^{-1}), and hence they cannot be distinguished.

Fig. 6 shows the ^{29}Si MAS-NMR spectra of as-synthesized and calcined GaMCM-48. It can be seen from this

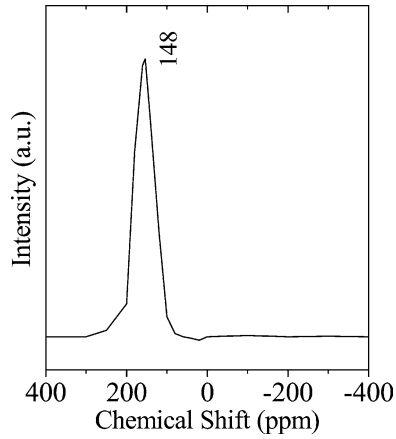

Fig. 7. ^{71}Ga MAS-NMR spectra of as-synthesized GaMCM-48.

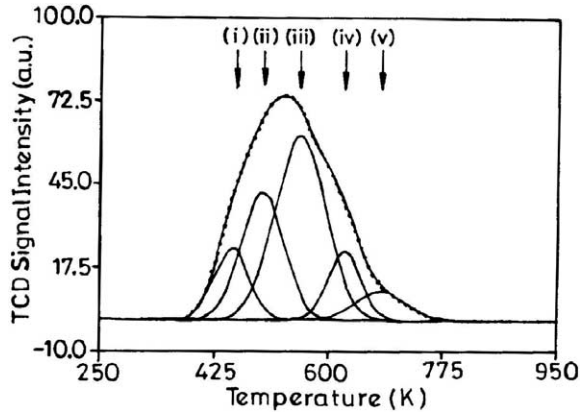

Fig. 8. Ammonia TPD profile of H-GaMCM-48.

figure that the as-synthesized sample (Fig. 6,a) shows two main signals centered at −108.5 ppm, assigned to Q_4 site [Si(OSi)$_4$], and −99.5 ppm, assigned to Q_3 site [Si(SiO)$_3$(OH)], with a weak shoulder at −90.1 ppm attributed to Q_2 site [Si(OSi)$_2$(OH)$_2$], respectively [40]. However, upon calcination, the intensity of Q_4 signal increases (Fig. 6,b), indicating further condensation of silanol groups resulting in the formation of siloxane (Si–O–Si) bonds. Fig. 7 depicts the ^{71}Ga MAS-NMR spectra of as-synthesized GaMCM-48, which shows a strong signal at 148.0 ppm corresponding to tetrahedral gallium, viz. Ga(OSiO$_3$)$_4$ and (HO)Ga(OSiO$_3$)$_3$, in the framework structure [9,20–22]. Indeed, similar ^{71}Ga MAS-NMR spectra have been reported for various Ga-substituted microporous [41,42] and mesoporous [20–23,43] molecular sieves.

Fig. 8 depicts the NH$_3$-TPD profile of H-GaMCM-48. The ammonia desorption trace was deconvoluted using a Gaussian function with temperature as variant. The first peak, around 420–440 K, referred to as type (i) is attributed to surface hydroxyl groups (weak acid sites; see Scheme 2) whereas the next two peaks, viz. type (ii) and type (iii), in the range 450–480 and 540–600 K originate from moderate and strong structural (Brønsted) acid sites, respectively, as due to the presence of tetrahedral gallium in two differ-

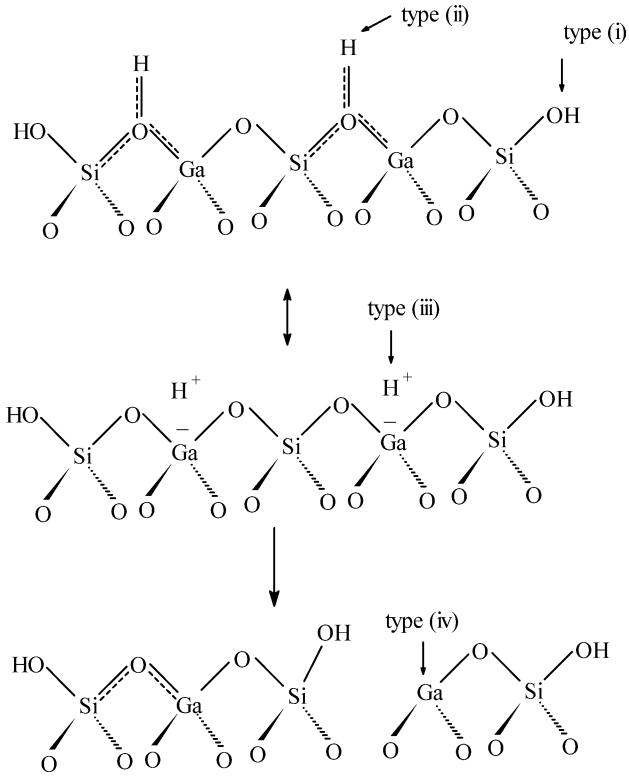

Scheme 2.

ent framework sites (see also Scheme 2). On the other hand, the broad and weak peak around 650–700 K, designated as type (iv), is attributed to weak Lewis acid sites, which may arise from tricoordinated gallium in the framework as illustrated in Scheme 2, and is also consistent with the results of ^{27}Al MAS-NMR and pyridine IR studies as well as the TPD [21,44]. However, a further increase in temperature (750 K) resulted in a weak peak, which may be assigned to corresponding nonstructural Lewis acid sites originating from the nonframework gallium species. An assignment of ammonia TPD peaks on the GaMCM-48 is based on others [21,28] and our previous reports [29,31,32]. Similar types of peak assignment were also reported for AlMCM-41 [21,44]. It is, however, clear from Fig. 8 that the area under the profiles corresponding to the moderate and strong Brønsted acid sites has a much larger contribution. Such a large amount of moderate-to-strong Brønsted acid sites (50–70%) is favorable for the chosen reaction.

Fig. 9 presents the results of *t*-butylation of phenol over H-GaMCM-48 under optimized experimental conditions (reaction conditions: $T = 448$ K; WHSV $= 4.8$ h^{-1}; TOS $= 1.5$ h; *t*-BA:phenol 2:1). For a comparison, we have also included the results of H-BMCM-41, H-AlMCM-41, H-GaMCM-41, H-FeMCM-41, H-BMCM-48, H-AlMCM-41, and H-FeMCM-48 [34]. It can be seen from this figure that, in general, the phenol conversion is higher for the MCM-48 structure than the corresponding MCM-41 structure. The observed high conversion of the former may, however, be explained on the basis of the following: (i) the three-

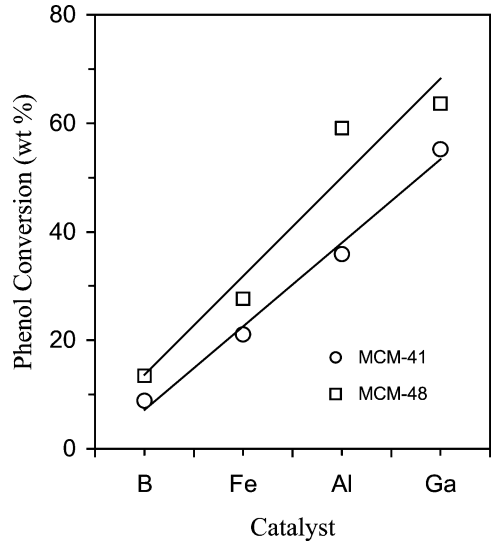

Fig. 9. Activity of various trivalent metal-containing mesoporous catalysts for the *t*-butylation of phenol reaction under optimized experimental conditions.

dimensional pore system of the MCM-48 structure (Fig. 9) favors more agitated flow because of its highly interwoven and branched pore structure, thereby increasing the number of interactions between reactant mixtures and catalytic sites than the one-dimensional pore system of the MCM-41 structure; see also Fig. 9 [7,12,19]; (ii) in addition, the MCM-48 structure possess a larger amount of moderate-to-strong Brønsted acid sites than the MCM-41 structure. On the other hand, as compared to the MCM-41 structure [29–32], the MCM-48 structure shows a slight decrease in *p*-*t*-butyl phenol selectivity at the expense of 2,4-di-*t*-butyl phenol.

Fig. 10 shows the effect of time-on-stream (TOS) on phenol conversion for different ratios of *t*-BA and phenol over H-GaMCM-48. It is clear from the figure that the catalyst does not show much deactivation. In contrast, the MCM-41-based catalysts show a deactivation of the catalyst [28–30], thus indicating that a three-dimensional pore system is more effective in the prevention of deactivation than a one-dimensional pore system. A similar analogy was made earlier for the vapor-phase isopropylation of naphthalene and pyrene over H-AlMCM-41 and H-AlMCM-48 [19]. At this juncture, it is also worth noting that a similar observation was also noted for the H-AlMCM-48 system [16]. Fig. 11 shows the effect of TOS on the phenol conversion over various mesoporous catalysts. There is no appreciable change in the phenol conversion over H-AlMCM-48 and H-GaMCM-48, indicating the absence of deactivation during the course of study. However, H-AlMCM-41 and H-GaMCM-41 show a slight deactivation. Thus this study also proves the advantages of a three-dimensional pore system over a one-dimensional pore opening for the chosen reaction. The effect of TOS on product selectivity over H-GaMCM-48 is shown in Fig. 12. It can be seen from this figure that no significant change in selectivity pattern of the products was observed.

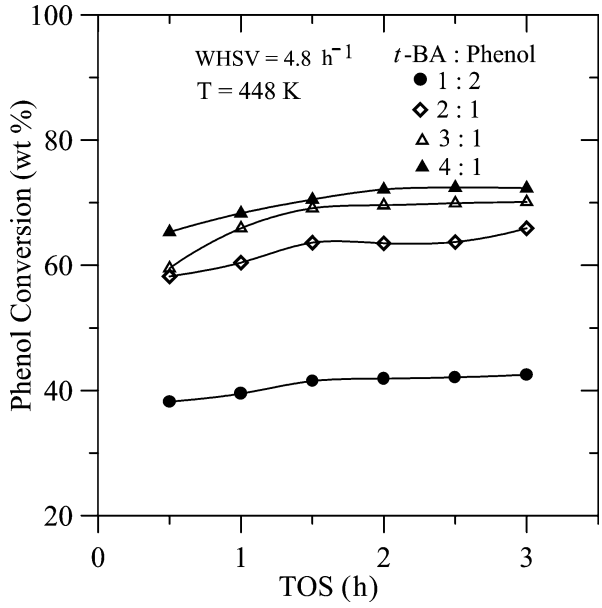

Fig. 10. Effect of TOS on the phenol conversion over H-GaMCM-48.

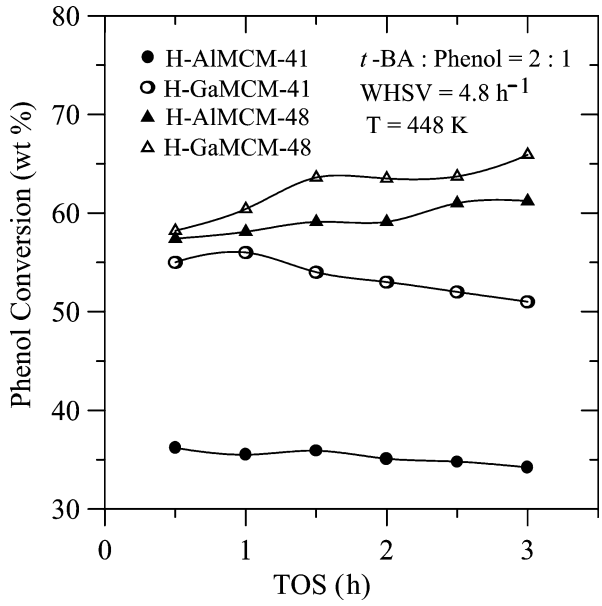

Fig. 11. Effect of TOS on the phenol conversion over various mesoporous catalysts.

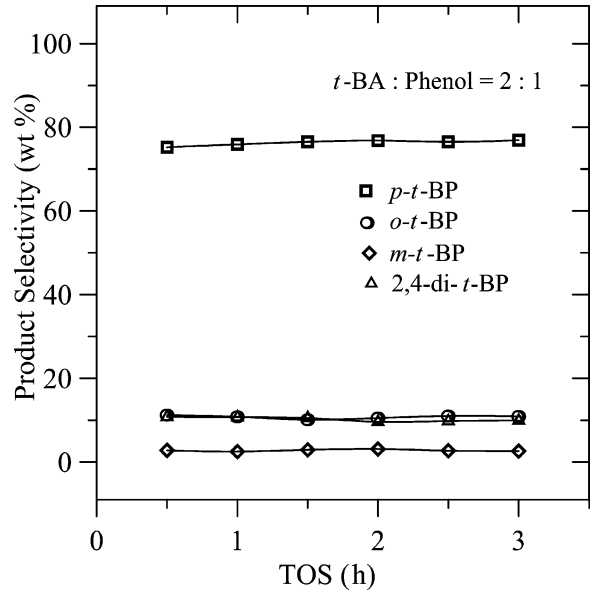

Fig. 12. Effect of TOS on the product selectivity over H-GaMCM-48.

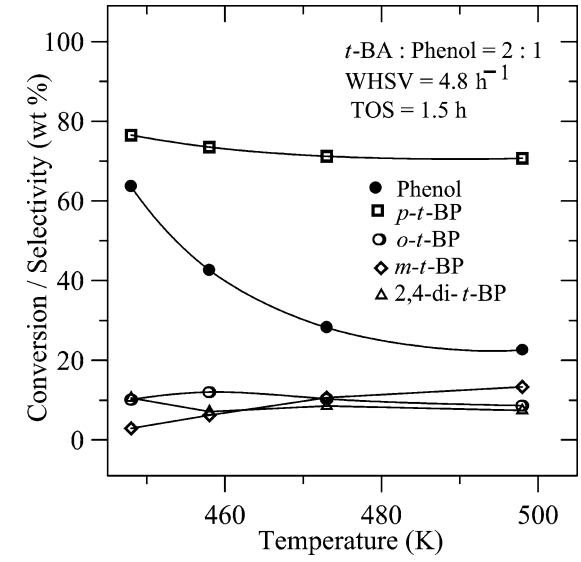

Fig. 13. Effect of temperature on the reaction over H-GaMCM-48.

Therefore, for further studies, an optimum molar feed mixture (*t*-butyl alcohol:phenol) of 2:1 molar ratio was chosen.

Fig. 13 depicts the effect of reaction temperature on the *t*-butylation over H-GaMCM-48. It can be seen from the figure that the phenol conversion decreases as the reaction temperature increases, which could be attributed to the dealkylation of *t*-BP [28,29]. Likewise, a slight decrease in *p*-*t*-BP and/or *o*-*t*-BP was noted with an increase in temperature, which could possibly be accounted for by the rearrangement of *o* and *p* products into thermodynamically favorable *m*-*t*-BP. A similar trend was also observed earlier for H-AlMCM-41 [29,30], H-FeMCM-41 [31], H-GaMCM-41 [32], and H-AlMCM-48 [16]. Further, a similar observation was reported earlier for alkylation of phenol with methanol over zeolite-Y [45]. Fig. 14 shows the effect of WHSV on the reaction. It is clear from this figure that with the increase in WHSV the substrate conversion decreases gradually. The observed higher conversion at low WHSV is due to the longer contact time of the reactant mixtures with the active sites of the catalyst. However, the lower conversion at higher WHSV could be due to the less contact time of reactant molecules. On the other hand, the increase in mono-alkylated products, viz. *p*-*t*-BP and *o*-*t*-BP, with an increase in WHSV, could be due to the absence of a secondary reaction as a consequence of less contact time of reactants/products with the catalyst.

Fig. 15 represents the effect of *t*-BA-to-phenol molar ratio on the *t*-butylation reaction over H-GaMCM-48. It can

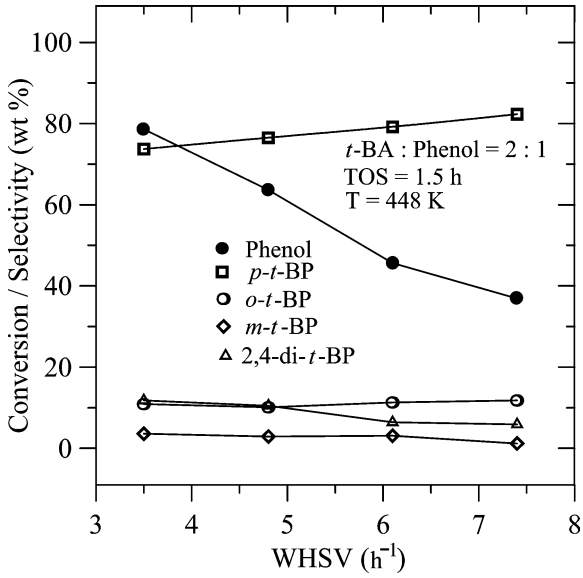

Fig. 14. Effect of WHSV on the reaction over H-GaMCM-48.

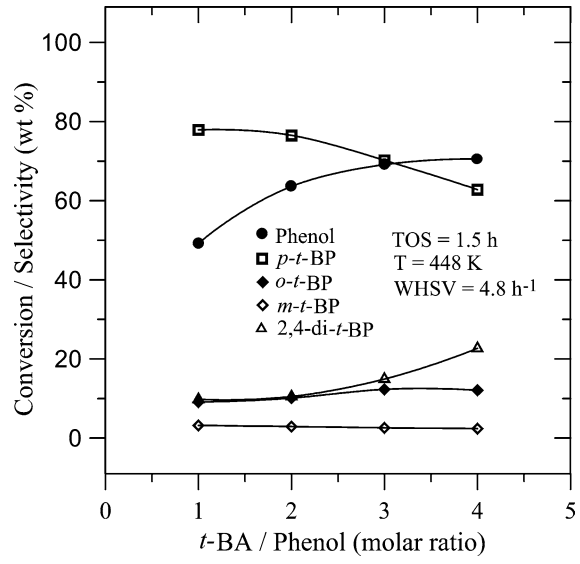

Fig. 15. Effect of *t*-BA-to-phenol molar ratio on the reaction over H-Ga-MCM-48.

be seen from figure that phenol conversion increases with an increase in *t*-BA-to-phenol molar ratio. This observation is in line with the literature [28] as the polar molecule such as methanol and higher alcohols compete with phenol for the adsorption sites, and with increasing molar excess of the alkylating agent, the phenol conversion increases. However, the increase in *t*-BA content leads to decrease in *p*-*t*-BP selectivity due to a possible secondary alkylation reaction resulting the formation of 2,4-di-*t*-BP. At this juncture, it is also worth noting that only a marginal or no activity was observed for the gallium-free siliceous MCM-48 as well as MCM-41.

4. Conclusion

In summary, in the present investigation, we have demonstrated the synthesis and characterization of high-quality mesoporous GaMCM-48 materials. Further, we have also shown that the protonated catalyst, viz. H-GaMCM-48, exhibits slightly higher activity for the *t*-butylation of phenol reaction than the H-AlMCM-48. However, it displays a much higher activity than the analogous B- and Fe-containing MCM-48 structure as well as the corresponding one-dimensional MCM-41 system. Moreover, the deactivation was found to be minimal owing to the three-dimensional pore opening, and hence displays superior catalytic performance. In addition, it was also deduced from this study that the increased activity of H-GaMCM-48 could be due to the presence of a large amount of moderate-to-strong Brønsted acid sites as compared to many other molecular sieve-based systems. Thus, in general, it is expected that the H-GaMCM-48 catalyst may show promise for acid-catalyzed reactions.

Acknowledgments

The authors thank RSIC/SAIF, IIT-Bombay for TEM, ^{29}Si MAS-NMR, and ICP-AES facilities, and instrumentation center, IISc, Bangalore for ^{71}Ga MAS-NMR. The authors also thank Dr. A. Sakthivel and Mr. F. Hussain for the initial work as well as for the experimental assistance.

References

[1] C.T. Kresge, M.E. Leonowicz, W.J. Roth, J.C. Vartuli, J.S. Beck, Nature 359 (1992) 710;
J.S. Beck, J.C. Vartuli, W.J. Roth, M.E. Leonowicz, K.D. Schmidtt, C.T.-W. Chu, D.H. Olson, E.W. Sheppard, S.B. McCullen, J.B. Higgins, J.L. Schlenker, J. Am. Chem. Soc. 114 (1992) 10834.
[2] A. Sayari, Chem. Mater. 8 (1996) 1840.
[3] A. Corma, Chem. Rev. 97 (1997) 2373.
[4] J.Y. Ying, C.P. Mehnert, M.S. Wong, Angew. Chem., Ind. Ed. Engl. 38 (1999) 56.
[5] D. Trong On, D. Desplantier-Giscard, C. Danumah, S. Kaliaguine, Appl. Catal. A 222 (2001) 299.
[6] P. Selvam, S.K. Bhatia, C. Sonwane, Ind. Eng. Chem. Res. 40 (2001) 3237.
[7] K.A. Koyano, T. Tatsumi, J. Chem. Soc., Chem. Commun. (1996) 145.
[8] W. Zhang, T.J. Pinnavaia, Catal. Lett. 38 (1996) 261.
[9] H. Kosslick, G. Lischke, H. Landmesser, B. Parlitz, W. Storek, R. Fricke, J. Catal. 176 (1998) 102.
[10] H. Landmesser, H. Kosslick, U. Kurschner, R. Fricke, J. Chem. Soc., Faraday Trans. 94 (1998) 971.
[11] X. Auvray, C. Petipas, R. Anthore, I. Rico, A. Lattes, J. Phys. Chem. 93 (1989) 7458.
[12] W. Zhao, Y. Luo, P. Deng, Q. Li, Catal. Lett. 73 (2001) 199.
[13] A. Sakthivel, S.E. Dapurkar, P. Selvam, Catal. Lett. 77 (2001) 155.
[14] A. Sakthivel, S.E. Dapurkar, P. Selvam, Appl. Catal. A 246 (2003) 283.
[15] S.E. Dapurkar, A. Sakthivel, P. Selvam, New J. Chem. 27 (2003) 1184.
[16] S.E. Dapurkar, P. Selvam, Appl. Catal. A 254 (2003) 239.
[17] K. Vidya, S.E. Dapurkar, P. Selvam, S.K. Badamali, D. Kumar, N.M. Gupta, J. Mol. Catal. A 181 (2002) 91, J. Mol. Catal. A 191 (2003) 149.

[18] E. Armengol, A. Corma, H. Garcia, J. Primo, Appl. Catal. A 149 (1997) 411.
[19] S.B. Pu, J.B. Kim, M. Seno, M.T. Inui, Micropor. Mater. 10 (1997) 25.
[20] C.-F. Cheng, H. He, W. Zhou, J. Klinowski, J.A.S. Goncalves, L.F. Gladden, J. Phys. Chem. 100 (1996) 390.
[21] H. Kosslick, G. Lischke, G. Walther, W. Storek, A. Martin, R. Fricke, Micropor. Mater. 9 (1997) 13;
H. Kosslick, H. Landmesser, R. Fricke, J. Chem. Soc., Faraday Trans. 93 (1997) 1849;
H. Kosslick, G. Lischke, B. Parlitz, W. Storek, R. Fricke, Appl. Catal. A 184 (1999) 49.
[22] K. Okumura, K. Nishigaki, M. Niwa, Chem. Lett. (1998) 749;
Micropor. Mesopor. Mater. 44–45 (2001) 509.
[23] R. Fricke, H. Kosslick, G. Lischke, M. Richter, Chem. Rev. 100 (2000) 2303.
[24] A. Sakthivel, P. Selvam, Bull. Catal. Soc. India 1 (2002) 41.
[25] E.H. Knozinger, J. Weitkamp, Handbook of Heterogeneous Catalysis, vol. 5, VCH, Weinheim, 1997;
J.H. Clark, D.J. Macquarrie, Org. Process. Res. Dev. 1 (1997) 149.
[26] K. Zhang, H. Zhang, G. Xu, S. Xiang, D. Xu, S. Liu, H. Li, Appl. Catal. A 207 (2001) 183.
[27] C.D. Chang, S.D. Hellring, US patent 5 288 927, 1994.
[28] S. Subramanian, A. Mitra, C.V.V. Satyanarayana, D.K. Chakrabarty, Appl. Catal. A 229 (1997) 159.
[29] A. Sakthivel, S.K. Badamali, P. Selvam, Micropor. Mesopor. Mater. 39 (2000) 457.
[30] S.K. Badamali, A. Sakthivel, P. Selvam, Catal. Today 63 (2000) 291.
[31] S.K. Badamali, A. Sakthivel, P. Selvam, Catal. Lett. 65 (2000) 153.
[32] A. Sakthivel, P. Selvam, Catal. Lett. 84 (2002) 37.
[33] S.E. Dapurkar, S.K. Badamali, P. Selvam, Catal. Today 68 (2001) 63.
[34] S.E. Dapurkar, PhD thesis, IIT-Bombay, 2004.
[35] E.P. Barrett, L.G. Joyner, P.P. Halenda, J. Am. Chem. Soc. 73 (1951) 373.
[36] R.D. Shannon, C.T. Prewitt, Acta Crystallogr. B 25 (1969) 925.
[37] K.S.W. Sing, D.H. Everett, R.A.W. Haul, L. Mosenu, R.A. Pierotti, J. Rouquerol, T. Siemieniewska, Pure Appl. Chem. 57 (1985) 603.
[38] R. Schmidt, M. Stöcker, M.D. Akporiaye, E.H. Tørstad, A. Olsen, Micropor. Mater. 5 (1995) 1.
[39] A. Carlsson, M. Kaneda, Y. Sakamoto, O. Terasaki, R. Ryoo, S.H. Joo, J. Electron Microsc. 48 (1999) 795.
[40] C.Y. Chen, H.-X. Li, M.E. Davis, Micropor. Mater. 2 (1993) 17.
[41] C.H.C. Timken, E. Oldfied, J. Phys. Chem. 109 (1987) 7669.
[42] E. Lalik, X. Liu, J. Klinowski, J. Phys. Chem. 96 (1992) 805.
[43] A. Tuel, S. Gontier, Chem. Mater. 8 (1996) 114.
[44] A. Sakthivel, S.E. Dapurkar, N.M. Gupta, S.K. Kulshreshtha, P. Selvam, Micropor. Mesopor. Mater. (2003), in press.
[45] S. Namba, T. Yashima, Y. Itaba, N. Hara, Stud. Surf. Sci. Catal. 5 (1980) 105.